# 行政院國家科學委員會專題研究計畫 成果報告

## 以發展新穎的乙醇轉化劑和陽極材料來製造出乾淨及高效率的乙醇固態氧化物燃料電池

## 研究成果報告(精簡版)

計 畫 類 別 ：個別型
計 畫 編 號 ：NSC 97-2113-M-003-006-
執 行 期 間 ：97 年 03 月 01 日至 98 年 07 月 31 日
執 行 單 位 ：國立臺灣師範大學化學系（所）

計 畫 主 持 人：王禎翰

計畫參與人員：碩士班研究生-兼任助理人員：毛永祥
碩士班研究生-兼任助理人員：詹少華
碩士班研究生-兼任助理人員：張軒誌
碩士班研究生-兼任助理人員：張亦甫
碩士班研究生-兼任助理人員：黃世昌

處 理 方 式 ：本計畫可公開查詢

中 華 民 國 98 年 09 月 17 日

# Final report (NSC97-2113-M-009-006-)

**Title**：From the Development of Novel Ethanol Reformer and Anode Materials to the Completion of the Clean and Highly Efficient Ethanol Solid-State Oxide Fuel Cell (SOFC)

**Principal Investigator**：Jeng-Han Wang (王禎翰)

**Sponsor**：National Science Council

**Keywords**：Ethanol reformer, solid oxide fuel cell (SOFC), first principles calculations

**Abstract**

The objective of this work is to develop better ethanol reformer and SOFC anode materials with the aim to design a better power generator by applying the efficient solid oxide fuel cell (SOFC) to directly utilize (or through internally reform) the clean and renewable ethanol fuel, the so-called ethanol SOFC. The advanced catalysts with excellent ethanol reforming efficiency and the superior electro-catalysts with good electrical conductivity and ethanol oxidation ability will be discovered to improve the power efficient, lower the fabrication cost and enhance the operational durability in the ethanol SOFC. Both the ethanol reformer integrated with hydrogen SOFC and the direct ethanol SOFC will be extensively studied and fully optimized to reach the best performance. The proposed power generator will have a much higher power density then typical combustion engines, be able to reduce the consumption of fossil fuels and reduce the green house $CO_2$ emission significantly.

This project will employ the hybrid experimental/computational approach in the studies of chemical synthesis, electrochemical measurements as well as mechanism elucidation. Initially, the promising ethanol reformers and SOFC materials will be synthesized and examined to determine the appropriate material compositions, morphologies and structures. The complete ethanol SOFC will be fabricated from these materials to test the system performance and optimize the operational condition. In addition, these experimental observations will be clearly understood from the detailed analysis of material properties and the comprehensive examination of reaction mechanisms. These fundamental studies, which will be systematically investigated by the *in situ* electrochemical measurement, *ex situ* materials characterization and first principles calculations, can help us construct the useful design rule to reduce the effort of experimental trial and error and speed up the discovery of novel materials in the ethanol SOFC application.

**Background:**

The limited oil resources and appreciation of the green house effect have led to the general public's awareness of the detrimental outcome from the world's addiction to fossil fuels and many governments' attention to exploring renewable energy resources and technologies. Most of the research has been focusing on the search for alternative energy resources with better "well-to-tank (WTT)" efficiency and new power generators with enhanced "tank-to-wheel (TTW)" efficiency with the aim to develop a superior system with the best "well-to-wheel (WTW)" efficiency along with less environmental impacts.

Among potential power generators, solid oxide fuel cells (SOFCs) can efficiently convert chemical energy to electricity without undesirable gas emission and have a great potential for future power generation. However, current development of SOFC requires purified hydrogen as fuel to avoid the degradation from carbon coking and sulfur poisoning in most hydrocarbon fuels. Although a variety of extensive studies for developing of novel SOFC materials with high coking and sulfur tolerance, it is not straightforward due to the intrinsic complexity of the interfacial phenomena of the electrochemical systems. In the searching of energy resources, hydrogen fuel has the advantages of non-pollution, in-exhausting and cost efficient and is considered as an excellent alternative energy source. Although hydrogen is a versatile energy carrier that is currently produced from variety of primary sources such as natural gas, heavy oil, alcohols, solar, wind and nuclear, the produced hydrogen is difficult and costly to store and transport in the present infra-structure. However, as summarized in Table 1, the studies still show a rather limited improvement at the current stage due to the fact that high WTT efficiency energy fuels cannot be fed to a suitable power generator and that the efficient SOFC can only utilize purified $H_2$ with low WTT efficiency [1].

Alternatively, ethanol, in particular, is an attractive energy source because of its high hydrogen content, availability, non-toxicity, as well as facile storage and handling safety, comparing with $H_2$, for example. The infrastructure and cost of ethanol production have become more mature and cheaper as the example of the increasing popularity of E85 fuel (with 85% ethanol) stations. On the other hand, SOFC, with better TWW efficiency than conventional combustion engines and without undesirable gas emissions, have been

considered as promising power generators [5-7].

**Table 1.** WTW, WTT and TTW of the energy resources and power generators in the present infrastructure.

| WTW | = | WTT [2] (production, storage and transportation) | × | TTW [3, 4] (Fueling operation) |
|---|---|---|---|---|
| $C_xH_y$ fuels < 22% | | < 84% *(high)* | | Combustion engine: < 16% *(low)*<br>Direct-hydrocarbon SOFC: < 25% *(low)* |
| $H_2$ fuel < 29 % | | Electrolysis, nuclear power < 58% *(low)* | | $H_2$-SOFC < 50% *(high)* |

**Objective:**

Our objective starts with the enhancement of ethanol reformer and SOFC fabrication and finalizes with the accomplishment of a functional ethanol SOFC, which employs the highly efficient SOFC to utilize the clean ethanol fuel. To achieve this objective, the materials is discovered by systematically optimizing the system performance of the ethanol oxidation and minimizing the carbon-poisoning behavior in the reforming and the SOFC performance is optimized in the $H_2$ environment by using sophisticated experimental techniques, *ex situ* characterization and *in situ* electrochemical measurement, in the material fabrication, performance testing, system characterization and intermediate identification. In addition, the reaction mechanism is extensively examined to help us scientifically screen the potential materials for fabrication and testing. The complicated heterogeneous reactions is solved by examining their elementary steps by advanced computational methods, first principles calculation, rate constant determination and thermodynamic correction, in the explaining of the experimental observation, understanding of the material properties and mechanism elucidation. The ethanol adsorption, C-C, C-O, C-H and O-H bond breaking reactions in the ethanol oxidation and the atomic carbon adsorption, carbon cluster formation, and $CO_2$ desorption in the carbon-poisoning reaction is taken into account in the mechanism study. These scientific studies can significantly accelerate the discovery of the better materials for the completion of ethanol SOFC.

**Previous works:**

In the study of the ethanol reforming, various metal-metal oxide catalysts, including the metals of Co, Ni, Cu, Ru, Rh, Pd, Pt and Ir supported on the metal oxides of $Al_2O_3$, $CeO_2$, $SiO_2$, $ZrO_2$, $TiO_2$, MgO, $La_2O_3$ and $Y_2O_3$, have been extensively studied as summarized in the recent reviews [8-10]. The result shows that the metals of Co, Ni, Ru and Rh can help for the carbon-carbon bond rupturing and the metal oxides of $CeO_2$ and $La_2O_3$ can enhance the oxidation process in the reforming of ethanol. Furthermore, Schmidt et al. have recently report the promising result of $Rh/CeO_2$ reformer [11], in which ethanol-water mixture can be converted to hydrogen with the selectivity about 100% and the conversion efficiency over 95%. Their result demonstrates that ethanol can be efficiently converted to hydrogen with an appropriate catalyst and resolves the essential problem of the costly hydrogen production and transportation.

Furthermore, the mechanistic studies of ethanol adsorption and decomposition on numerous metal surfaces, Pt(111) [12-15], Ni(111) [16], Pd(111) [17], Rh(111) [18, 19] and Au(111) [20] have been examined by first-principles calculations as well as by various experimental techniques, including X-ray photoelectron spectroscopy (XPS), IR spectroscopy, high resolution electron energy loss spectroscopy (HREELS) and temperature programmed desorption (TPD). These results show that ethanol can adsorb on the surface forming multilayer adsorbates at low temperatures and undergo dissociation and desorption at increasing surface temperature. The results [16, 18, 19] also show that Ni(111) and Rh(111) surfaces have better capabilities in decomposing the adsorbed ethanol than other metal surfaces. However, based on the decomposition result, the ethanol reforming mechanism is still not clear and the reforming activity cannot be rationally determined.

In the study of SOFC system, we intend to engage our efforts in fabrication and characterization of composite electrodes and electrolyte materials based on the most popular Ni/YSZ (Yttrium-stabilized zirconia)/LSM(Lanthanum Strontium Manganate) fuel cell system, in which the Ni/YSZ anode shows the most electrochemical stability in the pure $H_2$ fuel [21]. Recent works on the common Ni/YSZ/LSM SOFC have demonstrated a significant progress in the characterization of surface poisoning that follows the phase transformation of electrode materials upon exposure to carbon- and sulfur-containing gases, which may exist

in the ethanol reforming fuels [22, 23]. The results accurately predict the effective operational window, at different operational temperatures in various contaminant concentrations, for a typical SOFC with Ni-based anode.

**Method:**

**Computational method**: The calculations are performed using the Vienna *ab initio* Simulation Package (VASP) [24-26], at the density functional theory (DFT) level with 3D periodic boundary condition. The exchange-correlation function is treated by the generalized gradient approximation (GGA) [27] with Perdew-Wang 1991 (PW91) formulation [28]. Combining the accuracy of augmented plane waves with the cost-effective pseudopotentials implemented in VASP, the projector-augmented wave method (PAW) [29, 30] a method combining the accuracy of augmented plane waves with the cost-effective pseudopotentials, to establish a reliable *ab initio* computational framework., is applied in the basis set. The kinetic cutoff energy of 600 eV is employed and the Brillouin-zone (BZ) integration is sampled at about 0.05 × 2 (1/Å) intervals in reciprocal space by the Monkhorst-Pack scheme [31]. Higher cutoff energies and k-points values with smaller BZ sampling intervals are applied to examine the convergence of current calculations. The Nudged Elastic Band (NEB) method [32], simultaneously relaxing an interpolated chain of configurations between the initial and final positions to the minimum energy path, is employed to locate transition states in the ethanol decomposition reaction.

The solid surfaces of reformers and SOFC anodes are modeled by the repeated super cells with vacuum spaces in three directions. Repetition of the in-plane super cells creates an infinite slab, while the periodicity in the direction perpendicular to the slab creates an infinite stack of slabs, as shown in Figure 1. The plane-wave expansion in PAW method is included all plane waves with their kinetic energies smaller than the chosen 600-eV cut-off energy to ensure the convergence with respect to the basis set and the efficiency of the computational cost. Furthermore, the intrinsic properties of the materials are examined by the density of state analysis (DOS). The projected d-band distribution, the most contributed structures in the transition-metal-based catalysts, is compared to determine the chemical insight of the experimentally observed results.

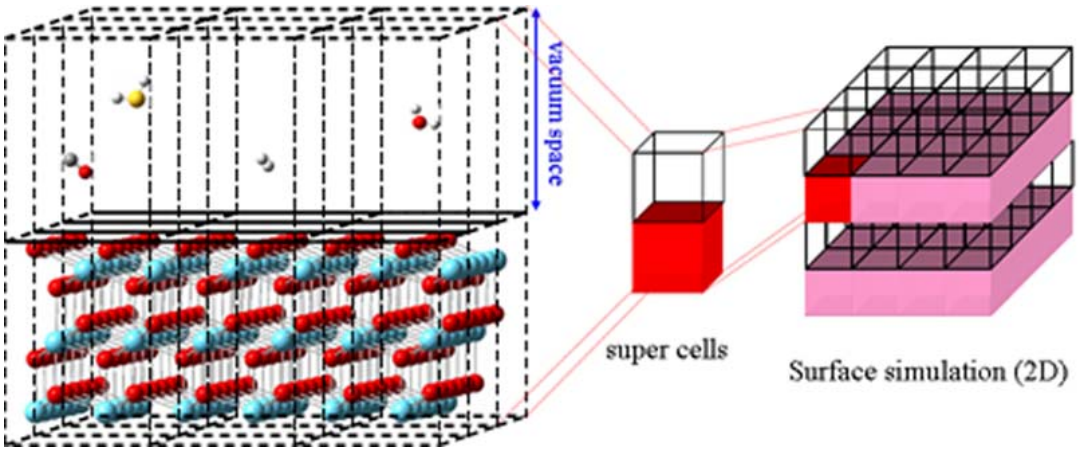


**Figure 1:** Illustration of slab model for interfacial reaction calculations.

**Reforming experiments:** The $CeO_2/Al_2O_3$ precursor is initially prepared by adding $Al_2O_3$ pellets, which the diameters are between 1.0mm and 1.4mm, in the solution of cerium nitrate(III) ($Ce(NO_3)_3{\bullet}6H_2O$) dissolved in de-ionized water. The precursor is dried in the oven at 100 °C and calcined in the furnace at 500 °C for 5 hours (in the air) to form $CeO_2/Al_2O_3$. The nine metallic catalysts of $M/CeO_2/Al_2O_3$, with the metal loading of 5 wt.% comparing to $CeO_2$ powder, are prepared by adding the supporter of $CeO_2/Al_2O_3$ in the aqueous solution of metallic salts, $Co(NO_3)_2{\bullet}6H_2O$, $Ni(NO_3)_2{\bullet}6H_2O$, $Cu(NO_3)_2{\bullet}3H_2O$, $RhCl_3{\bullet}xH_2O$, $PdCl_2$, $AgNO_3$, $IrCl_3{\bullet}xH_2O$, $H_2PtCl_6{\bullet}6H_2O$ and $HAuCl_4{\bullet}xH_2O$. The resulted reformers are reduced in $H_2$ at 600 °C for 2 hours.

The ethanol reforming system, as shown in Figure 2 includes the (1) pump system, which is equipped with mass-flow controllers for the carrier gas and an HPLC pump for the water/ethanol mixture with a desired ratio, (2) pre-heater, which is made of a stainless-steel vessel with an external heating tape and a temperature controller, (3) catalyst bed housing, which is a quartz tube with the synthesized ethanol reformer

inside and an external heating device outside the tube, (5) condenser, which is a simple water/ice bath, and (6) gas chromatography/mass spectroscopy (GC/MS) analyzer. The whole system is flexible and each part can be upgraded and changed easily for higher throughput or a range of catalysts with different compositions and dimensions.

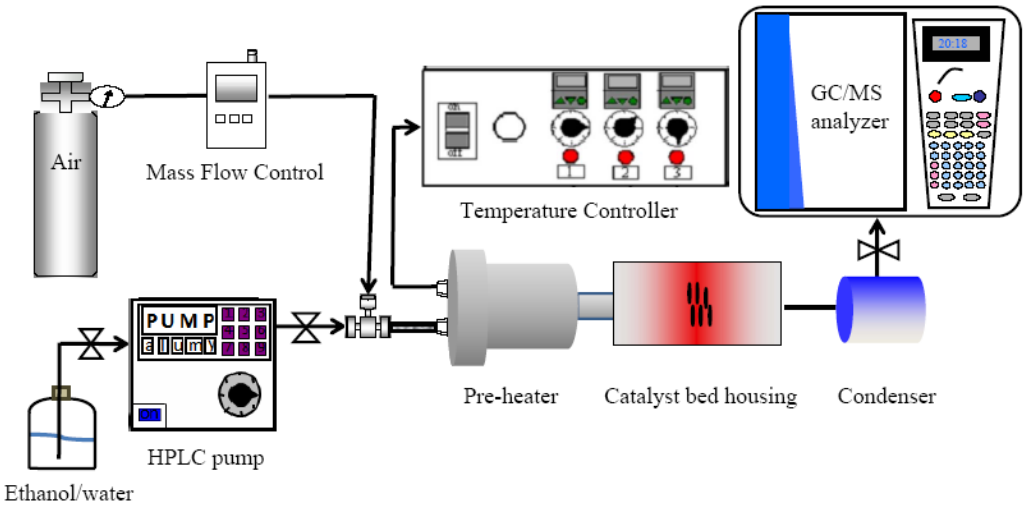


**Figure 2.** Schematic diagram of the ethanol reforming system

**SOFC experiments:** The SOFC system starts from the most electrochemical stable Ni/YSZ/LSM fuel cell system in the pure $H_2$ fuel. The fabricated SOFC systems are further optimized by modifying the anode composition, porosity ratios, electrolyte thickness operational conditions. The fabrication procedure of a button Ni/YSZ/LSM SOFC can be described in Figure 3 with following steps:
First, the metal oxide materials of anode, cathode and electrolyte are synthesis by glycine nitride process (GNP), in which mixing the metal nitride and glycine with the desired stoichiometry and firing at high temperature, to produce the fine powder with foam-like structure. Second, the thin porous anode/dense electrolyte membrane is fabricated by means of the simple and cost efficient co-pressing method. The porous electrode, the YSZ and NiO powder with a weight ration of 1 : 1 is mixed with flours and organic binder to form an anode precursor. The precursor is initially pressed at 200 MPa in a stainless steel mold, as a substrate, to flatten the surface and create certain mechanical strength. The dense electrolyte, a 10-µm-thick YSZ film, is formed by adding, uniformly distributing and uniaxially pressing the foam-structured YSZ powder, prepared by glycine-nitrate process (GNP) method, onto a the substrate of YSZ-NiO. The anode-supported anode/electrolyte bi-layer is subsequently sintered at 1400 $^oC$ for 5 hours, resulting in an YSZ (electrolyte) membrane on YSZ/NiO (anode) substrate. Finally, for cathode materials, conventional cathodes for oxygen ion conductor, Sr doped $LaMnO_3$ (LSM), is screen printed, a common method for preparation of uniform and porous cathode.

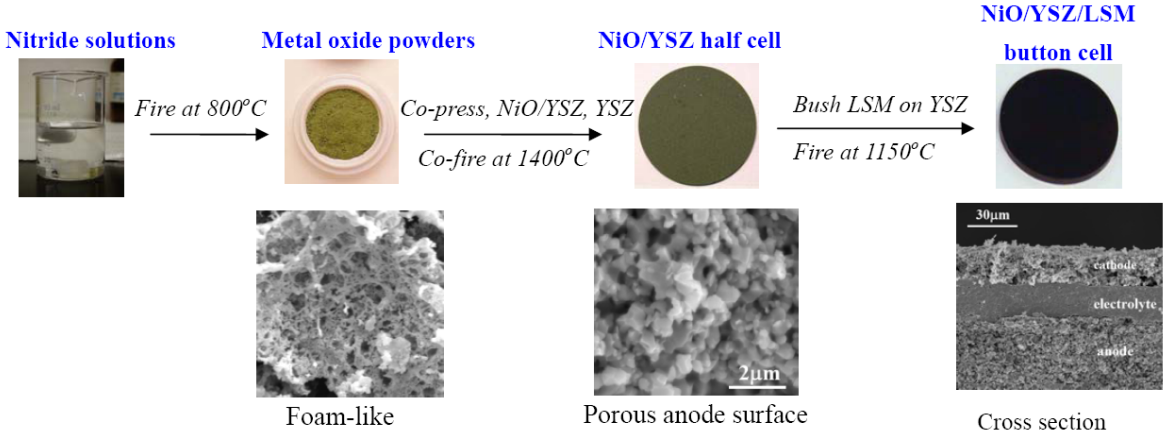


**Figure 3.** Fabrication procedures for a lab-scale Ni/YSZ/LSM cell

The electrochemical characterizations of functional cells is carried out by measuring the impedance spectra and power density, as described in Figure 4. Every cell is stabilized in $H_2$ at 750 $^oC$ for several hours before fuel cell tests are initiated. The SOFC performance is measured at 600 – 850 °C with both ethanol

reformed $H_2$ and purified ethanol as fuels and stationary air as the oxidant. The measurement is conducted in a cooling sequence, which is monitored by a Potentiostat/Galvanostat interfaced with an automated system.

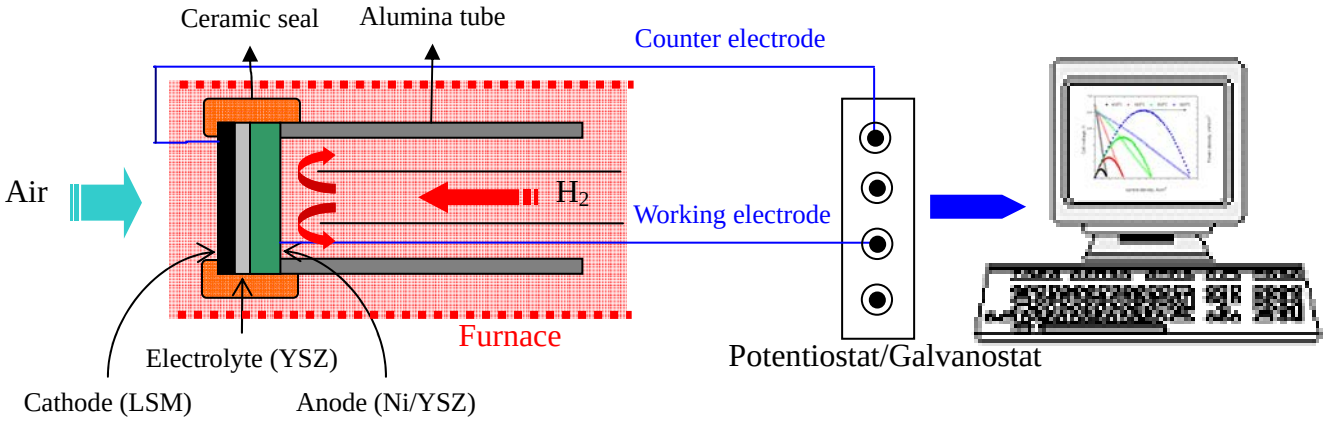


**Figure 4.** Schematic diagram of SOFC performance testing

**Results and discussion:**

**Ethanol reforming:** The nine selected metals of Co, Ni, Cu, Rh, Pd, Ag, Ir, Pt and Au and metal oxides of $Al_2O_3$, $CeO_2$, $ZrO_2$ and $SiO_2$ have been systematically examine to determine the reforming efficiency in different metal catalysts and metal-oxide supporters. The reforming efficiency of the possible combinations is listed in Table 2.

**Table 2:** The reforming efficiency (%) of the selected metals and metal oxides

| | Co | Ni | Cu | Rh | Pd | Ag | Ir | Pt | Au |
|---|---|---|---|---|---|---|---|---|---|
| $CeO_2$ | 20.2 | 27.3 | 20.3 | 90.5 | 26.9 | 15.0 | 97.3 | 53.7 | 17.6 |
| $ZrO_2$ | 2.8 | 0.3 | 9.7 | 41.0 | 12.5 | 5.1 | 61.4 | 15.1 | 7.1 |
| $SiO_2$ | 1.6 | 0.2 | 0.2 | 49.6 | 0.3 | 0.3 | 50.6 | 1.2 | 4.4 |
| $Al_2O_3$ | 2.6 | 1.7 | 5.5 | 50.0 | 12.8 | 2.7 | 56.6 | 20.8 | 11.6 |

The reforming result shows that Rh and Ir are considered as the best metal catalyst in all different supporters whereas Co, Ni and 1B group (Cu, Ag and Au) are considered as the worst ones. These results are consistent with previous experiments [9, 33-36]. Furthermore, our result shows that $CeO_2$ is considered as the best supports than the other three and the order of efficiency of metal catalyst might not be affected by the support although the supporter can enhance or decrease the efficiency of each metal catalyst.

Our experiment found another efficient reforming system, $Ir/CeO_2$. The efficiency if this system is similar to Schmidt's $Rh/CeO_2$ reformer [11], but with cheaper Ir catalyst. Furthermore, we optimize the reforming condition of C/O ratio and air flow (for contact time examination). Higher C/O can results over oxidation process and less one might be insufficient $O_2$ to react with ethanol. Therefore, a volcano curve can be expected. As shown in Table 3(a), the best C/O ratio is located at 0.6, which is between the best C/O ratio of Rh (0.7) and of Pt (0.5) and the volcano curve is plotted in Figure 5. The higher C/O ratio indicated that less $O_2$ join the reaction and ethanol decomposition is more likely to occur than oxidation. Therefore, more reforming $H_2$ might be resulted from the decomposition in Ru and $Ir/CeO_2$.

Similar, in the air flow testing, higher flow results less contact time on the catalytic surface and the reaction might be incomplete. On the other hand, lower flow causes longer reaction time and decreases reaction time. The result of air flow tests are shown in Table 3(b) and Figure 5 and the best air flow is located at 0.6 sccm. Compared with C/O ratio testing, the effect of air flow is relatively less important.

**Table 3:** The efficiency of $Ir/CeO_2$ system in several C/O ratios and air flows

| (a) C/O ratio | 0.4 | 0.5 | 0.6 | 0.7 |
|---|---|---|---|---|
| Efficiency (%) | 67.9 | 82.1 | 93.5 | 66.9 |

| (b) Air flow (sccm) | 0.5 | 0.6 | 0.7 |
|---|---|---|---|
| Efficiency (%) | 93.5 | 94.4 | 93.5 |

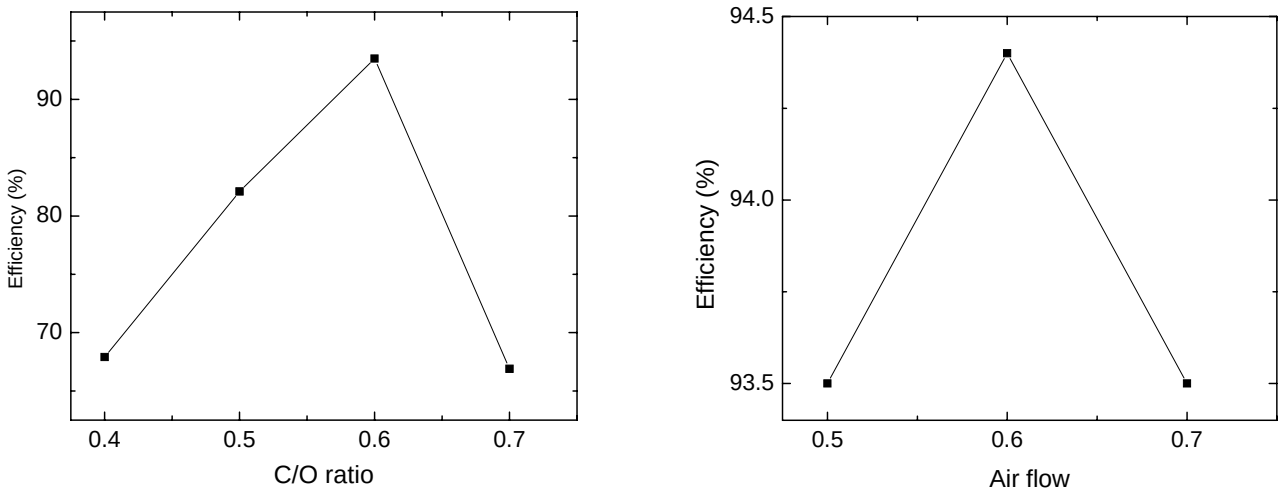


**Figure 5:** The volcano curve of reforming efficiency in different C/O ratios (left) and air flows (right)

Although a cheaper and efficient $Ir/CeO_2$ catalyst has been observed in the experiment, the detailed mechanism of ethanol reforming and the intrinsic property of reformer related to the efficiency are still unclear. To discover another catalyst might depend on luck and enormous try and error. Therefore, we intend to further determine the mechanism based on our results in the 36 combinations and assisted by the computational work.

The 4d to 6d catalysts of the groups 9 (Co, Rh and Ir), 10 (Ni, Pd and Pt) and 11 (Cu, Ag and Au) elements, which has been systematically studied in the experiment, have been examined in the current study. Since the structural effect, which the surface defects of steps, kinks or terraces could affect the dissociation barriers of catalytic reactions and the electronic structures of catalysts [37], might be similar on the metals with the same crystal structures [38, 39], the most stable (111) surface of the FCC catalysts has been employed for the current calculation.

The decomposition starts from the molecularly adsorbed ethanol with the most stable adsorption structure on the atop site [19], and follows by the initial C-C, C-O, C-H and O-H bond breaking processes, which lead to four possible routes in reactions (1), (2), (3) and (4), respectively

.

$$C_2H_5O(H)- \xrightarrow{TS(CC1)} H_3C-+-C(H_2)O(H)- \xrightarrow{TS(CO1)} H_3C-+H_2C-+HO- \quad (1)$$

$$C_2H_5O(H)- \xrightarrow{TS(CO2)} H_3C(H_2)C-+HO- \xrightarrow{TS(CC2)} H_3C-+H_2C-+HO- \quad (2)$$

$$C_2H_5O(H)- \xrightarrow{TS(CH1)} -C(H_2)C(H_2)O(H)-+H-\rightarrow$$
$$\begin{cases} \xrightarrow{TS(CC3)} H_2C-+-C(H_2)O(H)-+H- \xrightarrow{TS(CO3)} 2H_2C-+HO-+H- \\ \xrightarrow{TS(CO4)} -C(H_2)C(H_2)-+HO-+H- \xrightarrow{TS(CO3)} 2H_2C-+HO-+H- \end{cases} \quad (3)$$

$$C_2H_5O(H)- \xrightarrow{TS(OH1)} C_2H_5O-+H- \quad (4)$$

Furthermore, in reaction (4), the dissociated fragment of $C_2H_5O^*$ can further dissociate to form $H_3C^*$, $H_2C^*$, O* and H* following alike routes in reactions (5) - (7).

$$C_2H_5O^* \xrightarrow{TS(CC5)} H_3C^* + {}^*C(H_2)O^* \xrightarrow{TS(CO5)} H_3C^* + H_2C^* + O^* \quad (5)$$

$$C_2H_5O^* \xrightarrow{TS(CO6)} H_3C(H_2)C^* + O^* \xrightarrow{TS(CC6)} H_3C^* + H_2C^* + O^* \quad (6)$$

$$C_2H_5O^* \xrightarrow{TS(CH2)} {}^*C(H_2)C(H_2)O^* + H^* \longrightarrow \begin{cases} \xrightarrow{TS(CC7)} H_2C^* + {}^*C(H_2)O^* + H^* \xrightarrow{TS(CO7)} 2H_2C^* + O^* + H^* \\ \xrightarrow{TS(CO8)} {}^*C(H_2)C(H_2)^* + O^* + H^* \xrightarrow{TS(CC8)} 2H_2C^* + O^* + H^* \end{cases} \quad (7)$$

Finally, the fragments of $H_3C^*$ and $HO^*$ from earlier dissociation processes can completely decompose to form atomic C*, O*, and H* adsorptions via reactions (8) and (9), respectively.

$$H_3C^* \xrightarrow{TS(CH3)} H_2C^* + H^* \xrightarrow{TS(CH4)} HC^* + 2H^* \xrightarrow{TS(CH5)} C^* + 3H^* \quad (8)$$

$$HO^* \xrightarrow{TS(OH2)} O^* + H^* \quad (9)$$

The dissociation barriers of the transition states, TS(CC#), TS(CO#), TS(CH#) and TS(OH#) for C-C, C-O, C-H and O-H bond breaking processes, respectively, and the related activation of the each elementary step has been plot against with the d-band center of the metal catalyst, as shown in Figure 6.

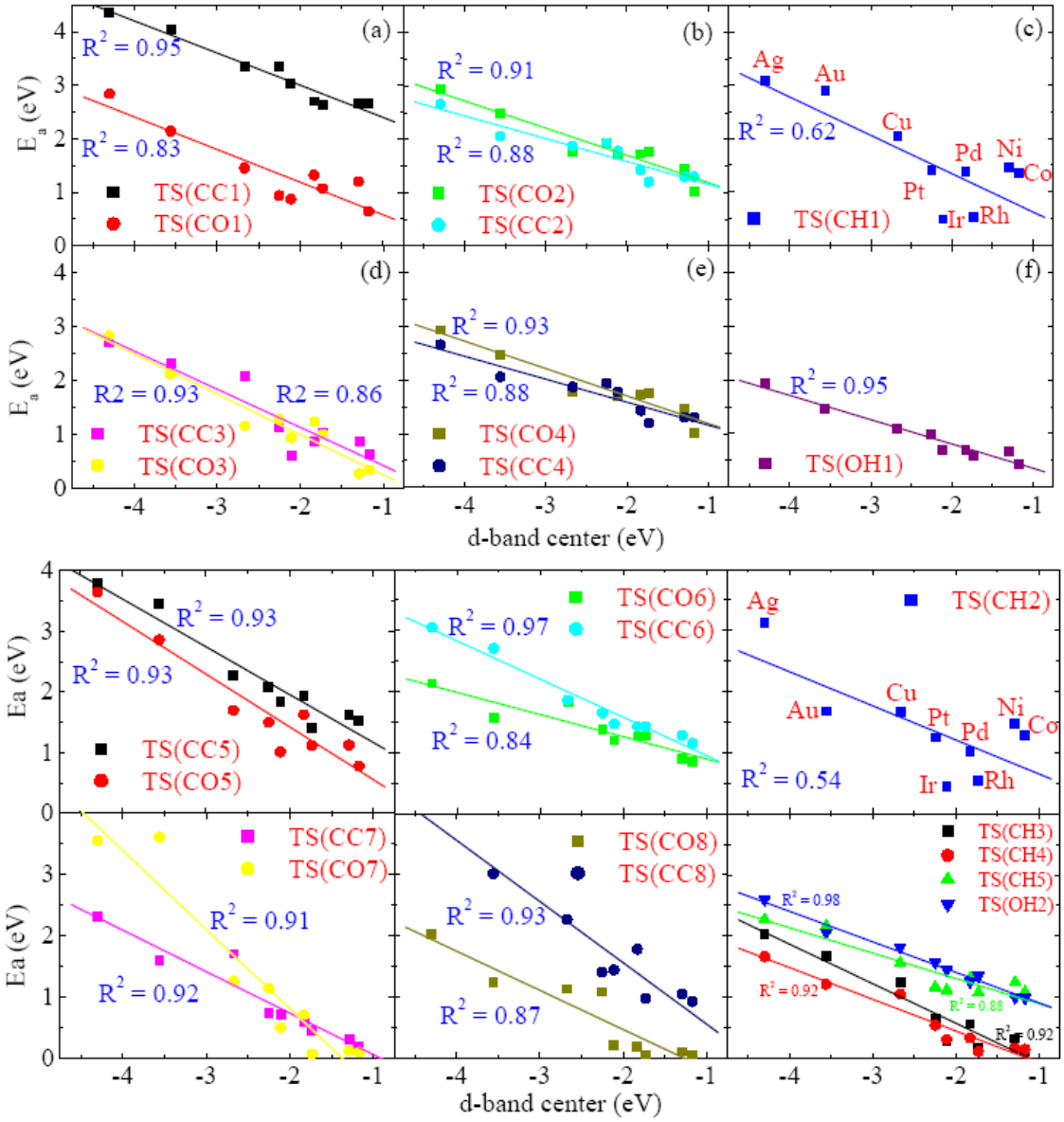


**Figure 6** The plot of the dissociation barriers in reactions (1) – (9) against the corresponding d-band centers of the nine selected metal surfaces.

Comparing the dissociation barriers of the elementary steps on the same metal surfaces, C-C bond breaking process has relatively higher dissociation barriers than the other C-O, C-H and O-H bond breaking processes. The initial C-C bond dissociation through TS(CC1) results the highest barrier on each metal and indicates that the ethanol decomposition is less likely to be occurred though reaction (1). Comparing reactions (2) and (3), the barrier of TS(CH1) is slightly lower than that of TS(CO2) and the following barriers of TS(CC3), TS(CC4), TS(CO3) and TS(CO4) in reactions (3) are relatively smaller than that of TS(CC2) in reaction (2). The result indicates that reaction (3) is considered as the most possible routes in ethanol decomposition and is supported from the experimental work [40], in which the double adsorption of $–C(H_2)C(H_2)O(H)-$ is observed as the key intermediate in the reforming reaction. In reaction (4), the dissociated fragment of $C_2H_5O-$ can further dissociate to $H_3C-$, $H_2C-$, O- and H- following the alike routes in reactions (1)-(3) with somewhat lower dissociation barriers, which can be attributed to the stronger adsorption energy of $C_2H_5O-$ and that of $C_2H_5O(H)-$. Similarly, the following C-H bond breaking process with the lower dissociation barrier of TS(CH2) to form $–C(H_2)C(H_2)O-$ is the most possible route for $C_2H_5O-$ decomposition and the following C-C bond breaking process through TS(CC5) has less chance to occur due to the high barrier. Finally, in the C-H bond breaking process of $H_3C*$, TS(CH3), TS(CH4) and TS(CH5) have lower barriers than those of TS(CH1) and TS(CH2) in the ethanol and $C_2H_5O*$ dissociation processes, respectively. The dissociation barrier of TS(CH5), which is higher than those of TS(CH3) and TS(CH4), is related to the stable HC* adsorption with greater adsorption energies (-6.4 ~ -3.6 eV) than those of $H_2C*$ (-4.3 ~ -2.4 eV) and $H_3C*$ (-2.0 ~ -1.4 eV), in consistence with the recent works on Pt(111), Rh(111), Pd(111) and Ni(111) surfaces [41-43]. Although the TS(CH5) has a slightly higher dissociation barrier, HC* can react with O*, which is expected to be present on catalyst surfaces during the reforming process, lowering its C-H bond dissociation barrier [41]. The result implies that atomic C and H adsorptions can occur easily on the surfaces once the ethanol is decomposed to $H_xC*$.

Comparing current decomposition calculation with previous reforming experiments, the computed result predicts that reactions (3) and (7) are the most likely pathways for ethanol reforming through the lower barriers of TS(CH1) and TS(CH2) forming the stable $*C(H_2)C(H_2)O(H)*$ and $*C(H_2)C(H_2)O*$ adsorbates, respectively; the result is in good agreement with the experimental observation that the doubly adsorbed five-member ring configurations are regarded as the key intermediates in the reaction [40]. In addition, the excellent performance of Rh- and Ir-based catalysts in the reforming experiments [8-11, 44] can be attributed to the geometrical effect which results in the lowest TS(CH1) and TS(CH2) barriers on Rh(111) and Ir(111) surfaces. Furthermore, the computed high dissociation barriers for the (111) surface of group 11 elements (Cu, Ag, Au) suggest poor catalytic properties for ethanol reforming and can well explain why these metals have infrequently been reported in the reforming experiments [8-10].

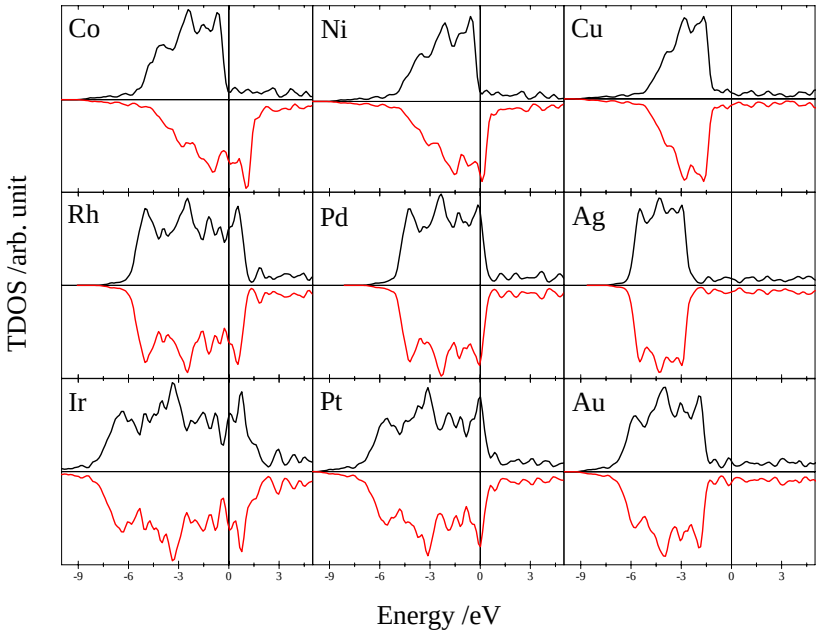


**Figure 7.** The total DOS of Co(111), Ni(111), Cu(111), Rh(111), Pd(111), Ag(111), Ir(111), Pt(111) and Au(111) surfaces.

Furthermore, the electronic structures of the selected metal surfaces have been examined from the density of state (DOS) analysis. Figure 7 shows the total DOS (mostly contributed from the metal d-band states) of spin α and spin β from group 9-11 metals with the same crystal structure and surface orientation. Comparing the DOS between 3d and 5d (row comparison in the periodic table), the upper 3d metals (Co, Ni and Cu) have more contracted DOS distribution and the lower 5d metals (Ir, Pt, Au) have more delocalized ones. Similarly, the distributions of the group 11 elements (Cu, Ag and Au) are more contracted than the metals in group 9 and 10. The shapes of DOS can be attributed to the nuclear-electron attraction that the upper-right elements in the periodic table have stronger attraction and result in more contracted distributions, which are closely related to the redox capability of catalytic metals. The delocalized DOS around the Fermi level, which can accept/donate electrons and act as electron reservoir in the redox reaction [45], can be considered as an indicator of redox capability of catalysts. On the other hand, the empty/filled electronic states near the Fermi level can accept/donate more electrons to enhance the reduction/oxidation reactions. Since these metals are conductive elements, their DOS are all continuous around the Fermi level. However, the surfaces of Rh(111) and Ir(111) show a much higher DOS distribution near the Fermi level and can be regarded as the more active catalysts for redox reactions in the reforming of ethanol. Cu(111), Ag(111) and Au(111) surfaces, in contrast, are relatively less active.

Considering both the computed decomposition barriers and DOS distributions, the (111) surfaces of group 11 elements (Cu, Ag, Au) are expected to be less efficient in the reforming of ethanol due to their high dissociation barriers and low DOS distributions near the Fermi level. On the other hand, Rh(111) and Ir(111) surfaces are anticipated to be the best ethanol reformers among these metals due to their low TS(CH1) and TS(CH2) barriers and high DOS distributions around the Fermi level. Furthermore, the better efficiency of Pt- and Pd-based reformers than Co- and Ni-based ones in the experiments [9, 33-36] can be understood from the slightly elevated barriers and the relative higher DOS distribution around the Fermi level on Pt(111) and Pd(111) than Co(111) and Ni(111) surfaces. This result may also indicate that the redox reaction plays a more important role than decomposition does in ethanol reforming. In addition, though Co(111) and Ni(111) surfaces have lower barriers, but with insufficient redox capability the rapid dehydrogenation process results in carbon poisoning on catalyst surfaces [37].

**SOFC:** Starting from the powder fabrication, the anode (NiO), cathode (LSM) and electrolyte (YSZ) materials are synthesized by $Ni(NO)_3.6H_2O$, $ZrOCl_2.8H_2O$, $Y(NO_3)_3$, $La(NO_3)_3.6H_2O$, $Sr(NO_3)_2$ and $Mn(NO_3)_2.4H_2O$. The XRD result shows that the fabircated samples show the desired peak and have no second phase. The firing temperature is ranged from 600 – 1000 $^oC$, and the particle size increases as the the firing temperature or time increases (Figure 8). Furthermore, the particle morphology has been analysized by SEM. The image shows that the excellent foam-like structure. Therefore, current GNP is suitable in our SOFC experiment.

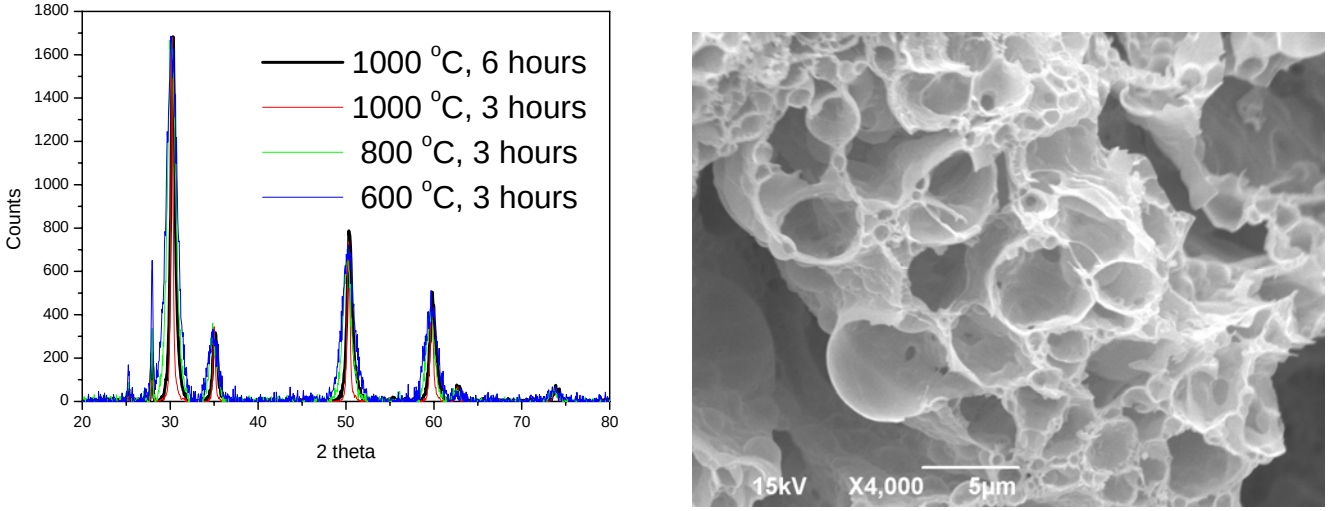


**Figure 8:** The XRD pattern at different firing temperatures and times (left) and the SEM image of the fabricated GNP powder (right)

The powders are further assembled as button cells for the electrochemical testing. Every cell is activated at 700 $^oC$ for 12 hours with $H_2$ purging in the anode. The activated cell has an ~ 1.0 V open circuit

voltage (OCV) in the temperature range of 700 – 900 $^{o}$C and slightly lower than the theoretical value of 1.23 V in the standard condition. After the OCV is raised to 1.0 V and stabilized for 12 hours, the power density of the cell has been measured in the linear voltage sweep (LVS) mode. As shown in Figure 9, the power density increases as the temperature increases and has slight improvement as the $H_2$ flow changed from 50 to 200 sccm. The result indicated that higher power density is resulted from the faster oxygen vacuum moving to enhance the ionic conductivity and reduce the internal resistant at higher temperature. On the other hand, since the anode has been activated in the $H_2$ environment over 12 hours and most of the NiO has been reduced to Ni in the anode, the $H_2$ flow has limited effect in the cell performance. The result also indicates that the active side of anode, triple phase boundary (TPB), has been saturated while $H_2$ is around 50 sccm.

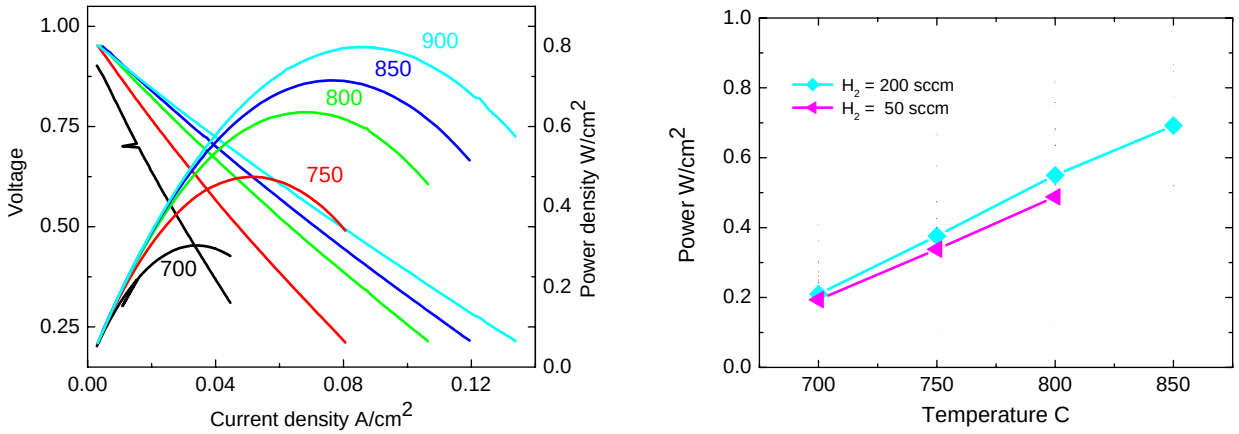


**Figure 9**: The power density of the button cell at different temperature (left) and with different $H_2$ flow.

**Summary and future work:**

In the ethanol reforming system, the mechanism of ethanol reforming has been systematically elucidated by the consistent experimental and computational works. The result shows that the best catalyst of Rh and Ir in the reforming experiment is related to the low ethanol decomposition barrier and high DOS distribution around the Fermi level in the first principles calculation. In the SOFC system, the cell fabrication procedure and test station have been successfully setup. Current result shows that the fabricated cell has an OCV around 1 V and the maximum power density is around 780 mW/cm$^2$ at 900 $^{o}$C.

The detailed mechanism study in the reforming system can help us intelligently design a better catalyst employed in both reforming and SOFC anode materials, the $H_2$-SOFC system setup is considered as the first and important step for the research of direct hydrocarbon SOFC with more convenience. Both of the techniques applied in our previous work might be useful in the searching for a better catalyst or electrocatalyst. In addition, this material study can be further improved by applying the high-throughput screening method in the current techniques to speed up the understanding of the catalytic mechanism and the discovery of the desired materials, as proposed in our new proposal.

**Self evaluation:**

Our work finished over 80% of the proposed work. The excellent reformer has been discovered, Ir/$CeO_2$, the detailed mechanism of ethanol reforming has been elucidated, and the SOFC system has been complete. These results have been published in one SCI journal and reported in two conferences. Furthermore, the searching for direct hydrocarbon SOFC anode is still under investigation and the research has been accelerate with the combinatorial technique.

**Journal and conferences**

1. **J. H. Wang**; C. S. Lee; M. C. Lin; Mechanism of Ethanol Reforming: Theoretical Foundations; J. Phys. Chem. C **113** 6681 (2009)
2. **J. H. Wang;** Catalytic Mechanism of Ethanol Reforming; Chinese Chemical Society Located in Taipei Annual Meeting, , Taiwan, December 7-8, 2008 (*Invited*)
3. **J. H. Wang;** The Material Development of Ethanol Reformers and Solid Oxide Fuel Cells in the Green Energy Research; Summer Workshop on Nanoscale Materials, Tainan, Taiwan, August 14-15, 2008 (*Invited*)

**Reference:**


(1) Haile, S. M., "*Nature Journal Club - Commentary on advanced anodes for solid oxide fuel cells*" *Nature* **2006,** 443, 375.
(2) Well-to-Wheel Energy Use and Greenhouse Gas Emissions of Advanced Fuel/Vehicle Systems. In General Motors, Argonne National Laboratory, BP, Exxon Mobile and Shell: 2001.
(3) "*Toyota Fuel Cell Hybrid Vehicle*" **2004**, http://www.toyota.co.jp/en/tech/environment/fchv/fchv11.html.
(4) Zhan, Z.; Barnett, S. A., "*An Octane-Fueled Solid Oxide Fuel Cell*" *Science* **2005,** 308, 844.
(5) Whittingham, M. S.; Savinell, R. F.; Zawodzinski, T., "*Introduction: Batteries and Fuel Cells*" *Chem. Rev.* **2004,** 104, 4243.
(6) Steele, B. C. H.; Heinzel, A., "*Materials for fuel-cell technologies*" *Nature* **2001,** 414, 345.
(7) Mclntosh, S.; Gorte, R. J., "*Direct Hydrocarbon Solid Oxide Fuel Cells*" *Chem. Rev.* **2004,** 104, 4845.
(8) Haryanto, A.; Fernando, S.; Murali, N.; Adhikari, S., "*Current status of hydrogen production techniques by steam reforming of ethanol: a review*" *Energy & Fuels* **2005,** 19, 2098.
(9) Navarro, R. M.; Pena, M. A.; Fierro, J. L. G., "*Hydrogen Production Reactions from Carbon Feedstocks: Fossil Fuels and Biomass*" *Chem. Rev.* **2007,** 107, 3952.
(10) Ni, M.; Leung, D. Y. C.; Leung, M. K. H., "*A review on reforming bio-ethanol for hydrogen production*" *Int. J. Hydrogen Energy* **2007,** 32, 3238.
(11) Deluga, G. A.; Salge, J. R.; Schmidt, L. D.; Verykios, X. E., "*Renewable hydrogen from ethanol by autothermal reforming*" *Science* **2004,** 303, 993.
(12) Lee, A. F.; Chang, Z.; Ellis, P.; Hackeet, S., F. J.; Wilson, K., "*Selective oxidation of crotyl alcohol over Pd(111)*" *J. Phys. Chem. C* **2007,** 111, 18844.
(13) Skoplyak, O.; Barteau, M. A.; Chen, J. G., "*Reforming of oxygenates for H2 production: correlaing reactivity of ethyl glycol and ethanol on Pt(111) and Ni/Pt(111) with surface d-band center*" *J. Phys. Chem. B* **2006,** 110, 1686.
(14) Wang, H.-F.; Liu, Z.-P., "*Selectivity of direct ethanol fuel cell dictated by a unique partial oxidation channel*" *J. Phys. Chem. C* **2007,** 111, 12157.
(15) Alcala, R.; Mavrikakis, M.; Dumesic, J., A., "*DFT studies for cleavage of C---C and C---O bonds in surface species derived from ethanol on Pt(111)*" *J. Catal.* **2003,** 218, 178.
(16) Xu, J. Z.; Zhang, X. P.; Zenobi, R.; Yoshinobu, J.; Z., X.; Yates Jr., J. T., "*Ethanol decomposition on Ni(111): observation of ethoxy formation by IRAS and other methods*" *Surf. Sci.* **1991,** 256, 288.
(17) Lee, A. F.; Gawthrope, D. E.; Hart, N. J.; Wilson, K., "*A Fast XPS study of the surface chemistry of ethanol over Pt{1 1 1}*" *Surf. Sci.* **2004,** 548, 200.
(18) Vesseli, E.; Baraldi, A.; Comelli, G.; Lizzit, S.; Rosei, R., "*Ethanol decomposition: C-C cleavage selectivity on Rh(111)*" *ChemPhysChem* **2004,** 5, 1133.
(19) Yang, M.-M.; Bao, X.-H.; Li, W.-X., "*First principles study of ethanol adsorption and formation of hydrogen bond on Rh(111) surface*" *J. Phys. Chem. C* **2007,** 111, 7403.
(20) Fartaria, R. P. S.; Freitas, F. F. M.; Silva Frenandes, F. M. S., "*A force field for simulating ethanol adsorption on Au(111) surfaces. A DFT study*" *Int. J. Quantum Chem.* **2007,** 107, 2169.
(21) Huang, Y.-H.; R. I. Dass; Xing, Z.-L.; Goodenough, J. B., "*Double Perovskites as Anode Materials for Solid-Oxide Fuel Cells*" *Science* **2006,** 312, 254.
(22) Wang, J. H.; Cheng, Z.; Brédas, J.-C.; Liu, M., "*Electronic and Vibrational Properties of Nickel Sulfides from First Principles*" *J. Chem. Phys.* **2007**, in press.
(23) Wang, J. H.; Liu, M., "*Computational study of sulfur-nickel interaction: A new S-Ni phase diagram*" *Electrochem. Comm.* **2007,** 9, 2122.
(24) Kresse, G.; Hafner, J., "*Ab initio molecular dynamics for liquid metals*" *Phys. Rev. B* **1993,** 47, 558.
(25) Kresse, G.; Hafner, J., *Phys. Rev. B* **1994,** 49, 1425.
(26) Kresse, G.; Furthmüller, J., "*Efficient iterative schemes for ab initio total-energy calculations using a plane-wave basis set*" *Phys. Rev. B* **1996,** 54, 11169.
(27) Cleperley, D. M.; Alder, B. J., *Phys. Rev. Lett.* **1980,** 45, 566.
(28) Perdew, J. P.; Yang, Y., *Phys. Rev. B* **1992,** 45, 244.
(29) Blöchl, P. E., "*Projector augmented-wave method*" *Phys. Rev. B* **1994,** 50, 17953.
(30) Kresse, G.; Joubert, D., "*From ultrasoft pseudopotentials to the projector augmented-wave method*" *Phys. Rev. B* **1999,** 59, 1758.
(31) Monkhorst, H. J.; Pack, J. D., "*Special points of Brillouin-zone integrations*" *Phys. Rev. B* **1976,** 13,

5188.
(32) Mills, G.; Jonsson, H.; Schenter, G. K., "*Reversble work transition state theory: application to dissociative adsorption of hydrogen*" *Surf. Sci.* **1995,** 324, 305.
(33) Breen, J. P.; Burch, R.; Coleman, H. M., "*Metal-catalysed steam reforming of ethanol in the production of hydrogen for fuel cell application*" *Appl. Catal. B* **2002,** 39, 65.
(34) Erdohelyi, A.; Rasko, J.; Kecskes, T.; Toth, M.; Domok, M.; Baan, K., "*Hydrogen formation inethanol reforming on supported noble metal catalysts*" *Catal. Today* **2006,** 116, 367.
(35) Fierro, V.; Akdim, O.; Mirodatos, C., "*On-board hydrogen production in a hybrid electric vehicle by bio0etanol oxidative steam reforming over Ni and noble metal based catalysts*" *Green Chem.* **2003,** 5, 20.
(36) Liguras, D. K.; Kondarides, D. I.; Verykios, X. E., "*Production of hydrogen for fuel cells by steam reforming of ethanol over supported noble metal catalysts*" *Appl. Catal. B* **2003,** 43, 345.
(37) Hammer, B.; Norskov, J. K., "*Theoretical surface science and catalysis - calculations and concepts*" *Adv. Catal.* **2000,** 45, 71.
(38) Liu, Z.-P.; Hu, P., "*General rules for predicting where a catalytic reaction should occur on metal srfaces: a density functional theory study of C-H and C-O bond breaking/making on flat stepped and kinked metal surfaces*" *J. Am. Chem. Soc.* **2003,** 125, 1958.
(39) Cheng, J.; Gong, X.-Q.; Hua, P.; Lok, C. M.; Ellis, P.; French, S., "*A quantitative determination of reaction mechanisms from density functional theory calculations: Fischer–Tropsch synthesis on flat and stepped cobalt surfaces*" *J. Catal.* **2008,** 254, 285.
(40) Sheng, P.-Y.; Yee, A.; Bowmaker, G. A.; Idriss, H., "*H2 production from ethanol over Rh-Pt/CeP2 catalysts: The role of Rh for the efficient dissociation of the carbon-carbon bond*" *J. Catal.* **2002,** 208, 393.
(41) Inderwildi, O. R.; Jenkins, S. J.; King, D. A., "*Mechanistic Studies of Hydrocarbon Combustion and Synthesis on Nobel Metals*" *Angew. Chem. Int. Ed.* **2008,** 47, 5253.
(42) Inderwildi, O. R.; Jenkins, S. J.; King, D. A., *J. Am. Chem. Soc.* **2007,** 129, 1751.
(43) Wang, S. G.; Liao, X. Y.; Hu, J.; Cao, D. B.; Li, Y. W.; Wang, J. G.; Jiao, H. J., *Surf. Sci.* **2007,** 601, 1271.
(44) Cai, W.; Zhang, B.; Li, Y.; Xu, Y.; Shen, W., "*Hydrogen production by oxidative steam reforming of ethanol over an Ir/CeO2 catalyst*" *Catal. Comm.* **2007,** 8, 1588.
(45) Liu, Z.-P.; Jenkins, S. J.; King, D. A., "*Origin and Activity of Oxidized Gold inWater-Gas-Shift Catalysis*" *Phys. Rev. Lett.* **2005,** 94, 196102.

附件一

# 行政院國家科學委員會補助專題研究計畫 ■ 成 果 報 告 □期中進度報告

From the Development of Novel Ethanol Reformer and Anode Materials to the Completion of the Clean and Highly Efficient Ethanol Solid-State Oxide Fuel Cell (SOFC)

計畫類別：■ 個別型計畫　□ 整合型計畫
計畫編號：NSC 97－2113－M－003－006－
執行期間：2008 年　3 月　1 日至　2009 年　7 月　31 日

計畫主持人：王禎翰
計畫參與人員：王禎翰，詹少華，張亦甫，毛永祥，張軒誌，黃世昌

成果報告類型(依經費核定清單規定繳交)：■精簡報告　□完整報告

本成果報告包括以下應繳交之附件：
□赴國外出差或研習心得報告一份
□赴大陸地區出差或研習心得報告一份
□出席國際學術會議心得報告及發表之論文各一份
□國際合作研究計畫國外研究報告書一份

處理方式：除產學合作研究計畫、提升產業技術及人才培育研究計畫、列管計畫及下列情形者外，得立即公開查詢
□涉及專利或其他智慧財產權，□一年□二年後可公開查詢

執行單位：國立臺灣師範大學化學系(所)

中　華　民　國　98 年　9 月　1 日

附件二

# 可供推廣之研發成果資料表

□ 可申請專利　□ 可技術移轉　　日期：__年__月__日

| | |
|---|---|
| **國科會補助計畫** | 計畫名稱：<br>計畫主持人：<br>計畫編號：　　學門領域： |
| **技術/創作名稱** | |
| **發明人/創作人** | |
| **技術說明** | 中文：<br>（100~500 字） |
| | 英文： |
| **可利用之產業及可開發之產品** | |
| **技術特點** | |
| **推廣及運用的價值** | |

※　1.每項研發成果請填寫一式二份，一份隨成果報告送繳本會，一份送　貴單位研發成果推廣單位（如技術移轉中心）。

※　**2.本項研發成果若尚未申請專利，請勿揭露可申請專利之主要內容。**

※ 3.本表若不敷使用，請自行影印使